Research Article Wiley Online Library ELECTROANALYSIS

doi.org/10.1002/elan.202100471

A Modulation QCM Applied to Copper Electrodeposition and Stripping

Christian Leppin,[a] Arne Langhoff,[a] Oliver Höfft,[b] and Diethelm Johannsmann*[a]

Abstract: A fast electrochemical quartz crystal microbalance with dissipation monitoring (EQCM–D) was applied to copper electrodeposition and subsequent stripping. Accumulation brings the frequency noise down to the mHz range, corresponding to 0.1 % of a monolayer. With this precision, the apparent mass transfer rate as determined from the time-derivative of the frequency shift can be directly compared to the current. Small but systematic deviations between the two can be attributed to nanoscale roughness. In the voltage range of underpotential deposition (UPD), the apparent mass transfer rate shows peaks and shoulders. The plating additive benzotriazole (BTA) leaves the magnitude of electrogravimetric signals unchanged, but shifts the UPD onset potential. The additive thiourea (TU) promotes UPD and strongly increases the bandwidth.

Keywords: Electrochemical Quartz Crystal Microbalance · EQCM · Electrodeposition · Modulation QCM, QCM(D) · Underpotential Deposition · Copper Electrodeposition · Plating Additives

1 Introduction

The electrochemical quartz crystal microbalance (EQCM) usually operates in the gravimetric mode and determines the change in mass per unit area of the electrode caused by electrodeposition or electroetching (stripping) [1,2,3,4,5,6,7,8]. In the simple cases, the mass transfer as determined with the QCM agrees with the mass transfer as calculated from the electrical current and Faraday's law [9]. The ratio of the two is the current efficiency. Side reactions can lower the current efficiency, while roughness and co-deposition can produce an apparent current efficiency larger than unity.

There are non-gravimetric effects at the lower end of the QCM's sensitivity range, caused by (among other effects) softness [8], roughness [10], slip [11], and the viscoelasticity of the double layer [12,13,14]. The interpretation of QCM data in terms of these effects is aided by analyzing the shift in half-bandwidth, $\Delta\Gamma$, in addition to the frequency shift, Δf, and, also, by including several overtones into the analysis [15]. Instruments providing this additional information are sometimes called QCM (D) for "QCM with dissipation monitoring".

A certain problem with the advanced QCMs is speed [16]. Analytical electrochemistry often exploits transients and the standard QCM(D)s have difficulties with data acquisition rates beyond 10 Hz. Fast data acquisition is easy and even natural with multifrequency lockin amplification. A multifrequency lockin amplifier (MLA) determines the entire resonance curve in a single shot with a frequency comb covering the resonance. The time resolution is equal to the inverse spacing of the frequencies of the comb, which must be less than the bandwidth of the resonance because the comb will otherwise miss the resonance. From this limit, it follows that the time resolution is a few milliseconds for measurements in liquids. The improved time resolution plays out its advantages when studying transient effects, as is common in analytical electrochemistry [17]. For one single measurement, fast data acquisition entails a correspondingly increased noise. The fast QCM does not beat the QCM's fundamental limits with regard to noise. However, accumulation and averaging will lower the noise if the process under study is repetitive. Cyclic voltammetry (undertaken with the QCM running in parallel) is among the suitable experimental settings. In the work reported below, accumulation overnight lowered the rms noise of $\Delta f/n$ down to 7 mHz, corresponding to a noise in mass per unit area of 0.12 ng/cm^2 for 5 MHz crystals (Δf and n are the frequency shift, and the overtone order, respectively). For comparison, the review by Ispas and Bund [18] reports a sensitivity of down to 1 ng/cm^2 (without accumulation, evidently). With $\rho = 8.96$ g/cm^3 as the density of copper, a noise in mass density of 0.12 ng/cm^2 translates to a noise in layer thickness of 0.14 pm.

[a] C. Leppin, A. Langhoff, D. Johannsmann
Institute of Physical Chemistry, Clausthal University of Technology, Arnold-Sommerfeld-Str. 4, 38678 Clausthal-Zellerfeld, Germany
E-mail: johannsmann@pc.tu-clausthal.de
[b] O. Höfft
Institute of Electrochemistry, Clausthal University of Technology, Arnold-Sommerfeld-Str. 6, 38678 Clausthal-Zellerfeld, Germany

Supporting information for this article is available on the WWW under https://doi.org/10.1002/elan.202100471

Accumulation not only improves the noise, it also avoids problems caused by instrumental drift. Resonator crystals drift in frequency at a rate of 1 Hz/hour or more because the crystal defects migrate. The drift can be circumvented by limiting the analysis to shifts in Δf and $\Delta\Gamma$ in response to some stimulus (to some modulation), rather than the absolute values of Δf and $\Delta\Gamma$. A modulation in this context is a repetitive change to the system parameters, to be synchronized with data acquisition. The absolute values still drift, but the difference from the average over the modulation period only drifts in proportion to the length of the modulation interval. We call this instrument a "modulation QCM". The modulation QCM is a QCM(D) insofar, as it reports frequency and bandwidth on a few overtones. The information gathered with this instrument goes beyond gravimetry. With regard to accumulation itself, AC-electrogravimetry [19] exploits the same principle.

Accumulation overnight raises the question, whether the properties of the sample remain constant over such long times. For the case of copper deposition and stripping, copper might gradually be dissolved in the gold electrode. It was tested, whether the first and the last cyclic voltammogram agreed. The peak current on the stripping peak stayed constant within 0.1 % (Figure S6 in the supporting information). Also, drifts in the absolute frequencies were monitored in parallel. The average of $\Delta f/n$ often decreased with a rate of about 1 Hz/hour. Given the instrumental drifts unrelated to deposition, this finding is not necessarily indicative of copper being dissolved in gold. If the instrument was more stable than it actually is, the slow decrease in $\Delta f/n$ might be interpreted as the consequence of an uptake of copper in the gold electrode.

It was also checked, whether the periodic transverse motion of the resonator surface would take an influence on the electrical current. An influence of vibrations onto electrochemical processes is exploited in sonoelectrochemistry [20,21]. The peak current on the stripping peak did not depend on the driving voltage of the resonator within 0.1 %, where the driving voltage was varied between 0 and 2 V (Figure S 5 in the supporting information). This EQCM is a linear device in the sense that the vibrating resonator only probes the electrochemical process under study without changing the current or the mass transfer rate.

Because of the good precision, the time derivative of $-\Delta f/n$ is determined with tolerable noise [22]. The time derivative of $-\Delta f/n$ is proportional to an apparent mass transfer rate and can therefore be directly compared to the current. Of course, the comparison may also be based on an integration of the current trace, leading to a charge per unit area. Integration is disadvantageous insofar, as the prime interest in electrochemistry usually is in the rate of the respective process under the chosen conditions, rather than the total amount of converted material. The rate is inferred from the current, not from the charge.

The example chosen to demonstrate the advantages and the limitations of the modulation QCM is copper electrodeposition and stripping. Copper electrodeposition is a process of much technical importance and has been studied in corresponding detail [23,24]. In the early 2000s, copper replaced aluminum as the interconnect metal in the semiconductor industry. At present, sulfate and fluoroborate solutions are the dominant electrolytes for electroplating, electroforming, and electrorefining [25]. Sulfate solutions were chosen here. The experiment covers both bulk deposition (left in Figure 1) and underpotential deposition (UPD, [26,27], right in Figure 1). UPD of copper on gold has been studied with the EQCM early after the EQCM was invented [6]. Few researchers have continued these studies because the instrument's noise ($\approx$1 Hz in Ref. [6]) is just slightly below the frequency shift induced by UPD [28]. Exploiting accumulation, we return to experiments of this kind, now being able to resolve more details.

In the case of the data reported below, the peaks and shoulders observed in the mass transfer rate and the current cannot be assigned to specific processes, based on QCM data and cyclic voltammetry alone. The experiment would have to be combined with structural investigations, for instance based on x-ray diffraction [29] or scanning tunneling microscopy [30,31,32]. Another problem is that the electrodes of a QCM are polycrystalline. Electrodes with single-crystal surfaces have been prepared on a QCM, but the effort is substantial [33 and references therein].

Technical electrodeposition is usually carried out in the presence of additives [34,35,36,37,38]. The plating additives benzotriazole (BTA) and thiourea (TU) were indeed found to affect both bulk deposition and UPD. BTA and TU may adsorb on the freshly forming Cu layer, causing an additional mass load. Again, it would require a

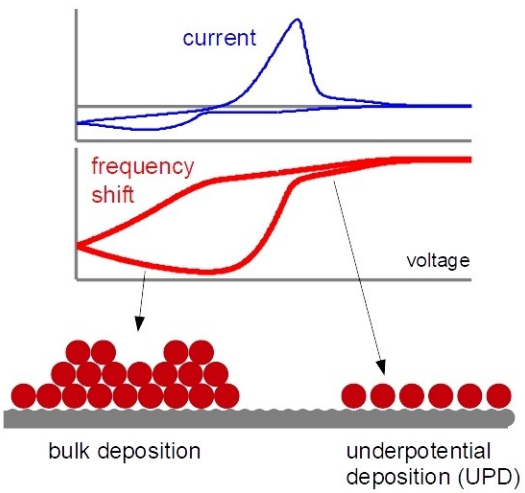

Fig. 1. Attractive interactions lead to a deposition of a submonolayer of copper on gold at a potential, which is more positive than the Nernst potential of the redox pair Cu^{2+}(aq)/Cu(s).

combination with structural investigations to assign the features reported in section 3.3 to specific processes.

The principal advantage of the modulation QCM is its precision. It reveals peaks and shoulders in plots of the mass transfer rate versus potential, similar to cyclic voltammetry. The integration time must be larger than in cyclic voltammetry, but otherwise the data quality is comparable. Electrogravimetry undertaken this way can play a role in electroanalytical chemistry similar to cyclic voltammetry and electrochemical impedance spectroscopy (EIS). It constrains the models and hints at certain explanations. The experimental effort is moderate.

1.1 Effects of Double Layer Viscoelasticity and Roughness

We briefly elaborate on the sources of non-gravimetric signals. For the configuration under study here (no soft films), the two most important sources are the viscoelasticity of the double layer and roughness. These two types of effects have at length been discussed by the Tel Aviv group [39 and references therein]. These were experiments with polarizable electrodes (no charge transfer across the electrode surface). It was not always possible to uniquely assign the shifts of Δf and $\Delta\Gamma$ seen in these experiments to either of the two sources.

From the canonical model for the response of the QCM to the deposition of a thin, planar, viscoelastic film [40,41,42,43,44], one infers the relation

$$\frac{\Delta_0 f + i\Delta_0\Gamma}{f_0} = -\frac{\omega}{\pi Z_q}\rho_{bulk}\int_0^\infty \left[\frac{\rho(z)}{\rho_{bulk}} - \frac{\eta_{bulk}}{\eta_{(z)}}\right] dz \qquad (1)$$

The subscript '0' in 'Δ_0' indicates a difference from a reference state, which is the semi-infinite liquid with no surface anomalies. (The letter 'Δ' without subscript further down denotes a difference from the average over the modulation cycle.) In the derivation of Eq. 1, a Taylor expansion of the more general result is employed. Eq. 1 only applies to thin layers, which can be metal deposits or the diffuse double layer. $\rho(z)$ and $\eta(z)$ are the density profile and the viscosity profile. f_0 is the frequency of the fundamental. Z_q is the shear-wave impedance of AT-cut quartz. The term in square brackets (the contrast function) on the right-hand side is complex because the viscosity is complex ($\eta = \eta' - i\eta''$). Eq. 1 can be rewritten as

$$\begin{aligned}\frac{\Delta_0 f + i\Delta_0\Gamma}{f_0} &= -\frac{\omega}{\pi Z_q}\rho_{bulk}\int_0^\infty \left[\frac{\rho(z)}{\rho_{bulk}} - \eta_{bulk}\frac{\eta'(z) - i\eta''(z)}{|\eta(z)|^2}\right] dz \\ &= -\frac{\omega}{\pi Z_q}\rho_{bulk}\int_0^\infty \left[\frac{\rho(z)}{\rho_{bulk}} - (J'(z) - iJ''(z))i\omega\eta_{bulk}\right] dz\end{aligned} \qquad (2)$$

In the last line, the layer's viscoelasticity has been expressed in terms of the viscoelastic compliance, $J(z)$. Eq. 2 shows that a nonzero $\Delta_0\Gamma$ is indicative of moderate elasticity. If $\eta'' \ll \eta'$, the second term in square brackets is real. If, on the other hand, $\eta'' \gg \eta'$, this term is imaginary, but close to zero. More precisely, this requires $\eta'' \gg \eta_{bulk}$. A metal deposit will not cause an increase in bandwidth even though it is an elastic material. Only a material with a moderate elastic modulus leads to $\Delta_0\Gamma > 0$. Some elasticity of the diffuse double layer is to be expected in the MHz range because the double layer contains a concentrated electrolyte solution.

Arguably, effects originating the diffuse double layer should be small for the experiments reported here because the Debye length is less than 1 nm. (The supporting electrolyte was H_2SO_4 at a concentration of 0.1 M).

A second source of non-gravimetric effects is surface roughness [10,45]. Roughness effects in EQCM experiments have been studied experimentally in Refs. [22,46,47]. In the latter two cases, the EQCM was combined with an AFM. Adapted to the geometry discussed here, shallow, nanoscale roughness affects the complex frequency shift as follows:

$$\frac{\Delta_0 f + i\Delta_0\Gamma}{f_0} = -\frac{1}{\pi Z_q}\omega\frac{h_r}{l_r}\frac{3\sqrt{\pi}}{2}\rho h_r + \frac{\sqrt{i\omega\rho\eta}}{\pi Z_q}2\left(\frac{h_r}{\delta}\right)^2 \qquad (3)$$

The reference state is the smooth surface immersed in a liquid with viscosity η and density ρ. h_r and l_r are a vertical scale and a horizontal scale of roughness, respectively. h_r/l_r is an aspect ratio, which may be assumed to vary less than the overall roughness. Approximating h_r/l_r as constant, the first term on the right-hand side has the structure of the Sauerbrey equation. It does not change the bandwidth, it predicts $-\Delta f/n$ to be constant, and it scales linearly with the height of the rough structure. This term covers trapped mass. Technically speaking, this term does not even describe a non-gravimetric effect. The QCM weighs the trapped liquid in addition to the metal itself. (Note the prefactor of $3\pi^{1/2}/2$, which is larger than unity.)

Changes in bandwidth come about by the term $2(h_r/\delta)^2$ on the right-hand side. δ is the penetration depth of the shear wave. The prefactor is proportional to the shear-wave impedance of the bulk liquid $Z_l = (i\omega\rho\eta)^{1/2}$. The shifts in frequency and bandwidth induced by the second term scale as $n^{3/2}$ because δ scales as $n^{-1/2}$. As noticed on an experimental basis in Ref. [48], the change in bandwidth induced by roughness often is smaller than the change in frequency. Eq. 3 corroborates this statement. Using $\rho = 1$ g/cm^3, $\eta = 1$ mPa s, $\delta = (2\eta/(\rho\omega))^{1/2} = 252$ nm, $f = f_0 = 5$ MHz, $h_r = 1$ nm, and $l_r \approx h_r$, the increase in half bandwidth is predicted as 0.02 Hz, while the decrease in frequency is 15 Hz.

The Tel-Aviv group has proposed a second model of roughness [10], which is applicable to high-aspect ratios (as opposed to shallow roughness). This model predicts a large increase in bandwidth. However, it also predicts a large deviation from Sauerbrey scaling for $\Delta f/n$, which is not found in the experiments reported here. For this

reason, we assume shallow roughness and analyze the data with Eq. 3. The bottom panel in Figure 5 from Ref. [22] (a line scan from an AFM image) and, also, Figure 2 in Ref. [47] (AFM images) support this assumption.

2 Materials and Experimental

2.1 Chemicals

All chemicals were used as received without further purification. $CuSO_4 \cdot 5\ H_2O$, thiourea, and sulfuric acid were obtained from Sigma-Aldrich (Sigma-Aldrich, St. Louis, United States) in a purity of $\geq 99.99\,\%$. Benzotriazole was obtained from Cofermin (Cofermin Chemicals, Essen, Germany). 2.5 mM solutions of $CuSO_4$ in 0.1 M sulfuric acid were prepared by dissolving $CuSO_4 \cdot 5\ H_2O$ in ultrapure water (resistivity ≥ 18.2 MΩcm) generated by an arium 611VF reverse osmosis system (Sartorius, Göttingen, Germany) and adding concentrated sulfuric acid. The solutions containing benzotriazole and thiourea as plating additives were prepared similarly. The concentration of the additive was 10 µM. The volume of the cell was 15 mL.

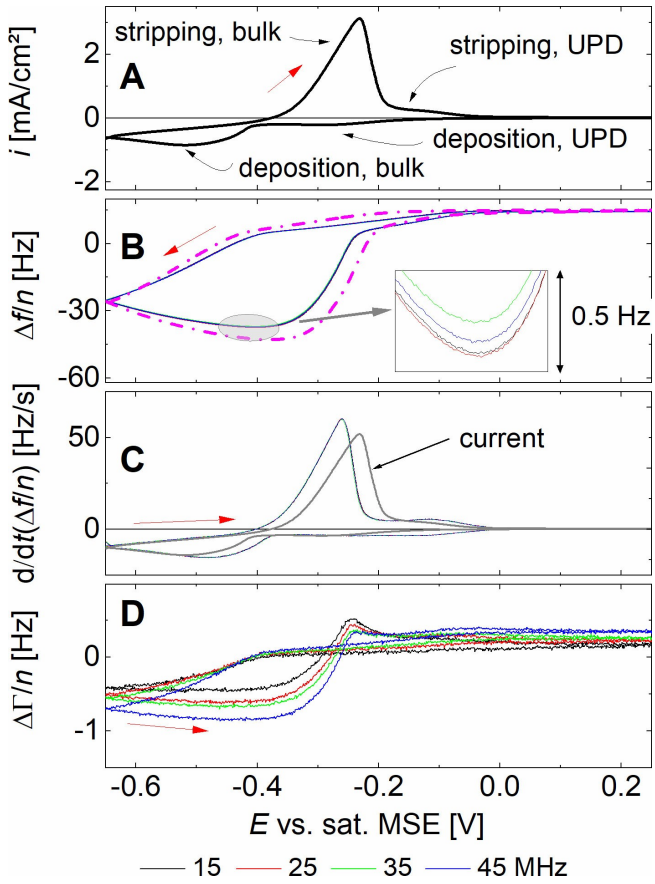

Fig. 2. A typical set of results. These data were obtained on a 2.5 mM solution of $CuSO_4$ in 0.1 M H_2SO_4. A: The current density shows the deposition and stripping features for both the bulk material and the UPD layer. B: Overtone-normalized frequency shifts on 4 overtones (15, 25, 35, and 45 MHz). The data from the different overtones overlap. The dash-dotted line is an equivalent frequency shift, calculated from the current with Faraday's law and the Sauerbrey equation. The inset shows a magnification of the minimum of the deposition peak, making the differences between the overtones visible. C: Time derivative of the frequency shift. The different overtones overlap. The time derivative is proportional to an apparent mass transfer rate. The grey line shows the current for comparison (same scale as in panel A). D: The overtone-normalized shifts in bandwidth, $\Delta\Gamma/n$, decrease while deposition proceeds. They go through a maximum at the stripping peak.

2.2 Electrochemical Quartz Crystal Microbalance

Gold-coated resonators with a fundamental frequency of 5 MHz and a diameter of 14 mm were supplied by Quartz Pro (Stockholm, Sweden). The holder was manufactured in-house. The temperature of the EQCM was $22 \pm 1\,°C$. The potential at the resonator's front electrode was controlled by a potentiostat Interface 1010E (Gamry Instruments, Warminster, United States). The area of the electrode as inferred from an optical image was 1.17 cm^2.

A three-electrode setup was employed, containing a platinum counter electrode and a Hg/Hg_2SO_4 reference electrode in saturated K_2SO_4 (sat. MSE, $E = 658$ mV vs. SHE). Between measurements, the resonators were rinsed with water, followed by repeated scans of cyclic voltammetry in 0.1 M sulfuric acid, until the current-voltage traces became stationary.

The chamber was not purged with nitrogen. Reduction of oxygen (either from the air or produced at the counter electrode) may contribute to the electrical current without leaving a trace in the QCM data. Oxygen reduction lowers the apparent current efficiency.

The resonators were driven by a multi-frequency lock-in amplifier (MLA) supplied by Intermodulation Products AB (Stockholm, Sweden) [14]. The difference in frequency between two members of a frequency comb was 100 Hz, which results in a time resolution of 10 ms. $\Delta f(t)$ and $\Delta\Gamma(t)$ were determined on four overtones at 15, 25, 35, and 45 MHz. "Δ" denotes the difference from the average over the modulation cycle (as opposed to the difference from the frequency and the bandwidth of some reference state). Before taking the time derivative, the data traces of $\Delta f/n$ were smoothed with a Savitzky-Golay filter (33 points, 2nd order). Smoothing did not shift the maximum of the stripping peak by more than 5 mV.

Ideally, one would always want to study UPD on single-crystal surfaces because the structural details do matter. Electrodes with single-crystal surfaces have been prepared on a QCM using a rather intricate scheme [33], but this method involves the use of a glue, which adversely affects the vibration modes. We chose to rather live with the gold surfaces as received from the supplier. These electrodes are grown by physical vapor deposition, which proceeds by island growth and leads to pancake-like patterns. Figure S1 in the supporting information shows an AFM image. The rms-roughness was 0.91 nm

(averaged over an area of 1 μm^2). Grazing incidence x-ray diffraction showed that about 75 % of the surface was composed of the Au(111) plane (section A2 in the supporting information).

3 Results and Discussion

3.1 Overview

Figure 2 shows a typical data set, taken on a 2.5 mM solution of $CuSO_4$ in 0.1 M H_2SO_4. The potential was swept between −650 mV and +300 mV vs. sat. MSE with a rate of 120 mV/s.

Panel **A** shows the current density, $i(E)$, as in cyclic voltammetry. The expected features are seen, which are bulk deposition and bulk stripping (to the left), and underpotential deposition (UPD) and underpotential stripping (to the right). XPS spectra taken on the UPD layer and the bulk layer are shown in the Supporting Information (Figure S2).

The full lines in Figure 2B are the overtone-normalized frequency shifts, $\Delta f/n$, for the overtones at 15, 25, 35, and 45 MHz. The different overtones are not actually discernible as separate lines because the overtone scaling closely follows the Sauerbrey prediction. $\Delta f/n$ is almost the same on all overtones. Differences exist, but are unsystematic in the sense that they do not monotonically depend on overtone order. The inset expands a section of the graph to show the differences. If these differences were related to viscoelasticity or roughness, they would show a systematic trend, but they do not. A possible reason for these unsystematic differences are compressional-wave effects. The vibration modes have flexural admixtures, which take a small and complicated influence on Δf. We do not further analyze these small deviations from the Sauerbrey prediction.

The dash-dotted line in panel **B** is the equivalent frequency shift derived from the current, $\Delta f_{el}(E)$. The current was integrated to yield a charge. The charge was converted to a frequency shift with Faraday's law and the Sauerbrey equation [49]. The absolute values in this conversion are slightly uncertain because the potentiostat determines the total current (integrated over the area), while the QCM determines the mass per unit area. The conversion requires a precise knowledge of the electrode area ($A = 1.17$ cm^2 as determined from an optical image) and it also requires the current density to be the same everywhere on the electrode. The absolute values agree between QCM measurements and cyclic voltammetry to the expected degree. The curves differ in shape, discussed in more detail in section 3.2. As the EDX data shown in Figure S4 in the Supporting Information, deposition and stripping are fully reversible. The electrode surface is free of copper after cycling.

Figure 2C shows the time derivatives of $\Delta f/n$, proportional to an apparent mass transfer rate. The thin grey line shows the current (same as in panel **A**) for comparison.

Figure 2D shows the overtone-normalized shifts in bandwidth, $\Delta\Gamma/n$. This is a non-gravimetric effect and it clearly is systematic. (Non-gravimetric effects were unsystematic for $\Delta f/n$.) $\Delta\Gamma/n$ is much smaller than $\Delta f/n$ on all overtones. The overtone scaling in $\Delta\Gamma$ does not follow Sauerbrey, which is expected because $\Delta\Gamma$ is not connected to mass transfer. Part of this effect may be attributed to double layer viscoelasticity. The viscoelasticity of the diffuse double layer is dominated by SO_4^{2-}. The sulfate concentration is 100 mM (to be compared to Cu^{2+} with a concentration of 2.5 mM). Sulfuric acid is the supporting electrolyte. The viscosity B-coefficients of SO_4^{2-} and H^+ are 0.206 L/mol and 0.068 L/mol, respectively. The viscosity B-coefficient quantifies the fractional change in viscosity caused by the addition of the respective ion [50]. Given that the B-coefficient of sulfate is much higher than that of the proton, its influence on viscoelasticity is dominant. The B-coefficient applies to the limit of small concentration and it only describes viscosity, not viscoelasticity at MHz frequencies. Still, the B-coefficient is related to intermolecular interactions. If one out of a few different ions has the largest B-coefficient and this ion is present in large concentration, it can be expected to dominate the MHz viscoelasticity [14].

Attributing the changes in $\Delta\Gamma/n$ to sulfate depletion in the double layer alone is problematic insofar, as this effect should depend on the electrode potential, only. In experiment, however, the magnitude of the shifts in $\Delta\Gamma/n$ follows the deposition kinetics. It keeps decreasing while the voltage is swept upwards, as long as the deposition proceeds (lower left in Figure 2B). This behavior would typically be interpreted as either a decreased roughness of the copper layer or as a stiffening of the gold electrode by a reversible alloying with Cu. Roughness effects are in conflict with Eq. 3, which predicts changes in bandwidth to be small.

This decrease in $\Delta\Gamma/n$ was seen in strictly all experiments of this study. Ref. [22], on the contrary, finds a small increase in bandwidth upon copper deposition. Ref. [47] finds a sizeable increase in 3 out of 4 experiments and slight decrease in the 4th case. In view of these conflicting results, the decrease of $\Delta\Gamma/n$ should be interpreted with caution.

There is an overshoot in $\Delta\Gamma/n$ on the right slope of the stripping peak. This may be caused by a large concentration of copper ions close to the electrode surface, when the copper layer is rapidly dissolved. Cu^{2+} has a large viscosity B-coefficient (0.360 L/mol). The high concentration of copper ions may cause some elasticity of the diffuse double layer.

3.2 Bulk Deposition, Dependence on Sweep Rate

Figure 3 shows data similar to Figure 2 for a number of different sweep rates. The scans look similar. The plot is also meant to demonstrate the reproducibility.

The dashed line shows the equivalent of a copper monolayer (−18.2 Hz).

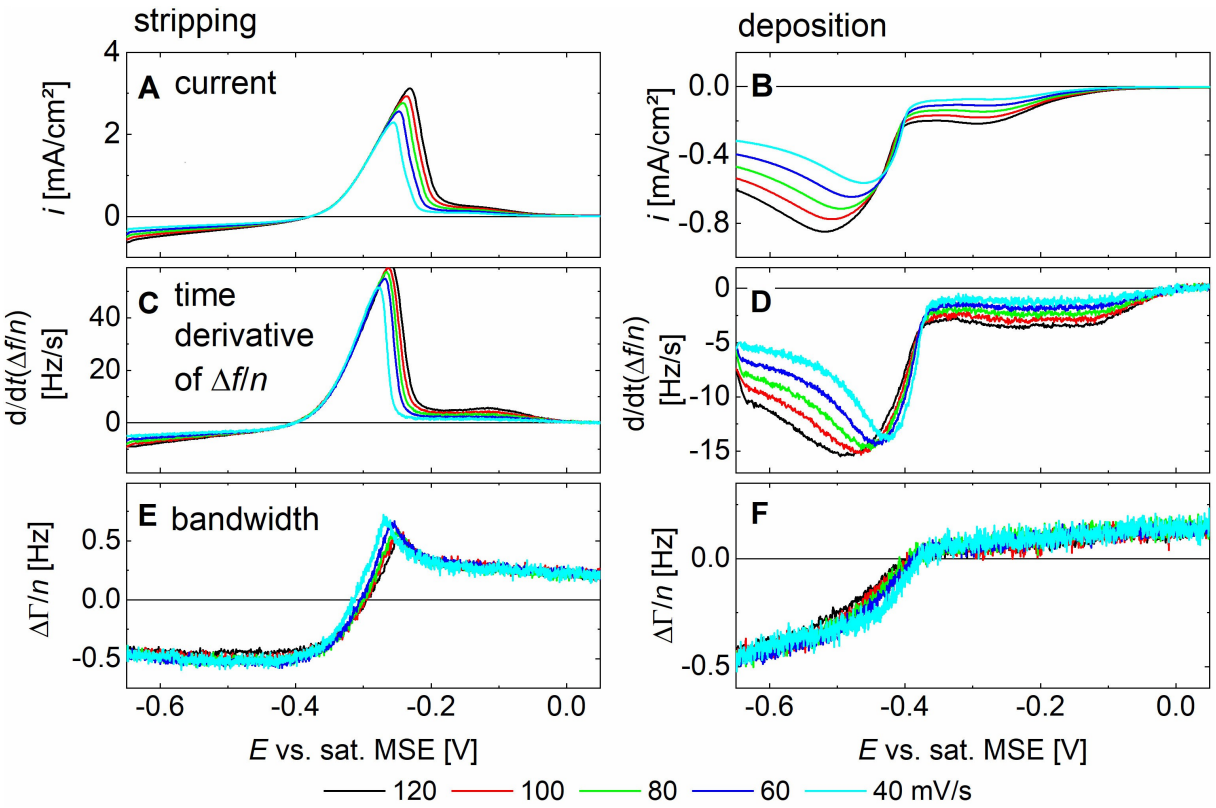

Fig. 3. Electrogravimetric sweeps at different rates. The sample was a 2.5 mM solution of $CuSO_4$ in 0.1 M H_2SO_4. Data from the overtone at 15 MHz are displayed.

Figure 4 extracts differences in $\Delta f/n$ from Figure 3, which pertain to bulk deposition and UPD. The contributions are inferred from plots of Δf vs. voltage as sketched in the inset. The amount of bulk material deposited per sweep increases with decreasing sweep rate because of the increased time per sweep. The amount of material deposited in UPD, on the contrary, does not depend on sweep rate. The value is $\delta_{UPD}(\Delta f/n) = -8.15 \pm 0.34$ Hz (mean ± standard deviation). This is less than half of the value, which would have been expected for a dense monolayer. The latter value is −18.2 Hz (for its calculation see section **D** in the supporting information). The amount of copper in the UPD layer is less than what would be expected from pseudomorphic growth. The lattice parameters of gold and copper are 407.82 pm and 361.48 pm, respectively [51,52]. Multiplying −18.2 Hz (the equivalent of a monolayer) by the square of the ratio yields a value of −14.3 Hz. Interpreting this deviation in detail would have to be speculation.

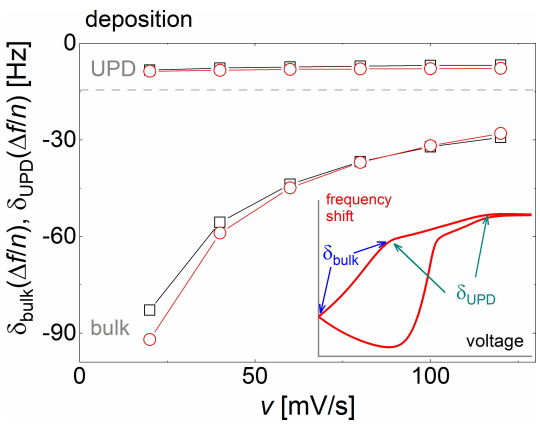

Fig. 4. Shifts in $\Delta f/n$ corresponding to UPD and bulk deposition as a function of sweep rate. These differences were extracted from plots of $\Delta f/n$ versus voltage as sketched in the inset. □: QCM data, ○: equivalent frequency shifts calculated from the electric charge. The sample was a 2.5 mM solution of $CuSO_4$ in 0.1 M H_2SO_4.

Figure 5 shows a test for the applicability of the Randles-Sevcik equation [55], typically used in cyclic voltammetry on redox couples in solution (as opposed to electrodeposition). For diffusion-controlled processes, the Randles-Sevcik equation predicts the peak current as $i_P = C\, v^{1/2}$, with C a constant depending on the diffusivity, the concentration, and the charge of the ion. As Figure 5 shows, the Randles-Sevcik relation only holds for the electric current in deposition, which makes sense because this process is limited by diffusion. For the other data sets (peak current on the stripping peak, time derivatives of $\Delta f/n$ on both peaks), the Randles-Sevcik plot leads to straight lines, but the fits can only be accomplished with a

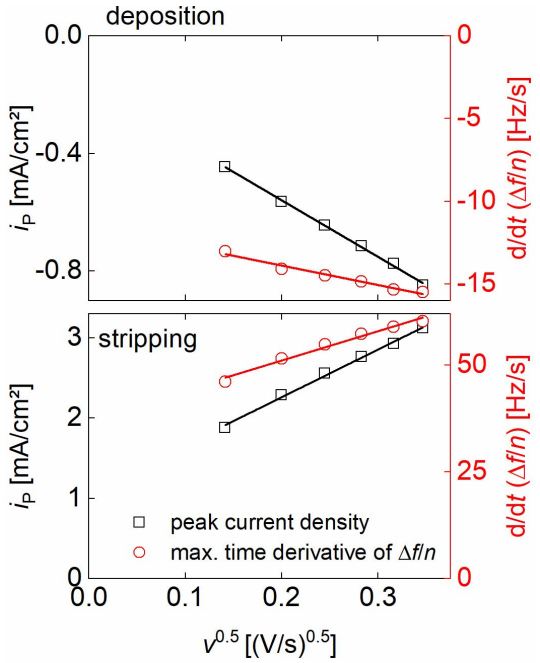

Fig. 5. A test for the applicability the Randles-Sevcik equation. The current and of the time derivative of $\Delta f/n$ on the peaks are plotted versus the square root of the sweep rate.

sizeable offset. With regard to current, such offsets have, for instance, been discussed in Ref. [56]. They are related to rate-determining processes other than diffusion. For the QCM data, the offset is much larger than for the current. This can be explained by roughness being larger for small deposition rates.

Figure 6 addresses the differences between the current and the apparent mass transfer rate. The peaks and steps are displaced from each other in all cases (bulk and UPD, deposition and stripping). On the potential scale, the displacements have opposite sign for deposition and stripping. The QCM responds earlier than cyclic voltammetry. We are not aware of a simple explanation for this finding. Viscoelastic effects are an unlikely explanation because the sign does not match the experiment. The Cu^{2+} ion has a large viscosity B-coefficient. Its rapid dissolution should increase the viscosity close to the resonator surface, thereby decreasing the frequency, However, the frequency is more positive than the equivalent frequency calculated from the charge (see also Figure 2B).

An explanation of the delay between apparent mass transfer rate and current with nano-scale roughness must include a mechanism explaining that the QCM responds earlier than cyclic voltammetry. Such a mechanism is sketched in Figure 7. Roughness may be particularly strong in the initial phase of nucleation, and it may be particularly weak in the late stages of electroetching because etching is most efficient at the tops of the asperities.

The peak positions of the current and the apparent mass transfer rate always differ. Values for bulk deposition and bulk stripping at various scan rates are reported in section E in the supporting information. The differences are larger in deposition than in stripping.

3.3 Underpotential Deposition with and without Additives

Underpotential deposition depends on the details of the interactions between the adsorbed ion and the substrate. Cyclic voltammetry shows multiple peaks, which ideally can be assigned to certain adsorptions sites and reactions, possibly involving solute molecules and counter ions [29].

Figure 8 shows potential sweeps similar to Figure 2, but limited to the UPD range. With one exception (inset

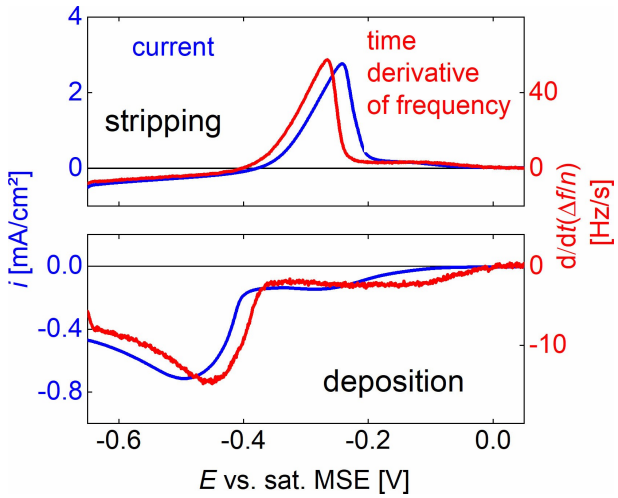

Fig. 6. A comparison between the current trace and the time derivative of $\Delta f/n$. The sweep rate was 80 mV/s. This is a subset of the data from Figure 3.

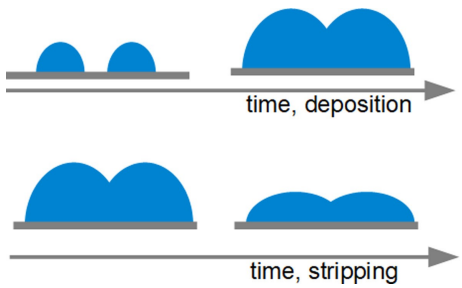

Fig. 7. If the differences between current and apparent mass transfer rate shown in Figure 6 are to be explained with roughness, a mechanism must be conceived, which lets roughness effects be strong in the initial phase of deposition and weak in the last stage of stripping. Roughness may decrease during deposition, when neighboring clusters merge. It may also decrease during stripping, when material is removed from the protrusions first, because the electric field is strongest there. In both cases, the time evolution of the charge is delayed with respect to the trapped mass.

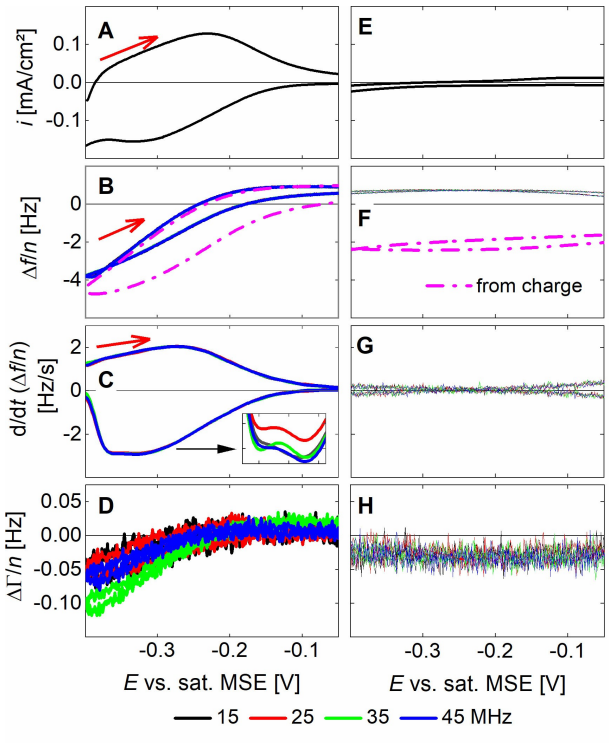

Fig. 8. Left: Data analogous to the data from Figure 2, where the sweep range was limited to the UPD range. Right: An analogous experiment, where the electrolyte does not contain copper. A and E: Current density. B and F: Frequency shift $\Delta f/n$. C and G: Time derivative of $\Delta f/n$. D and H: Bandwidth shift $\Delta\Gamma/n$.

in **C**), there are no peaks separated by minima. Presumably, the features are superpositions of different peaks, corresponding to the different crystal facets. In order to show more details (as reported in Ref. [26] for current traces), single-crystal surfaces would be needed.

Figure 9 shows potential sweeps at different sweep rates and compares the results obtained without additives to experiments, where BTA or TU had been added to the electrolyte in a concentration of 10 µM. Figure 10 shows the data set with rate of 120 mV/s together with the electric current and the bandwidth.

BTA leaves the bandwidth largely unchanged. It leaves the magnitude of the UPD unchanged, but it shifts the shoulder in the mass transfer rate to more negative potentials, so that it overlaps with the shoulder in current. (The shoulders in the apparent mass transfer rate and in the electric current are separate in Figure 10A.) The influence of BTA on copper electrodeposition was studied as early as 1991 by Armstrong and Muller, using an STM [53]. These authors report that crystallization of copper was inhibited by BTA. Leung et al. in 2000 used an AFM to study the effects of BTA on copper deposition [38]. They report reduced roughness. This finding may correspond to our findings insofar, as BTA in Figure 10B shifts the shoulder of UPD deposition, such that it coincides with the shoulder of the current (differently from panel **A**). A caveat: Being motivated by application, most studies on the effects of additives are concerned with bulk deposition at high rates. Transferring these findings to the UPD range may miss some aspects of UPD.

Thiourea as a widely used additive in copper deposition and has been studied numerous times. In 1985, Farmer studied copper UPD in the presence of thiourea, using electrochemical impedance analysis (EIS) [54]. He reports a large effect of TU on the high-frequency peak in the EIS spectra, which he interprets as the consequence of co-adsorption. Later work finds evidence for complexes between TU and copper [36] and, also, for the formation of CuS [37]. Upadhyay and Yegnaraman report that TU promotes UPD, which we can confirm. The frequency shift attributed to UPD was increased to 16.8 Hz, in the presence of TU (to be compared to 8.15 Hz in the absence of TU, section 3.2), which is close to the frequency shift expected for a copper monolayer (18.2 Hz). We also find an increased softness in presence of TU. More precisely, there is a layer with moderate elasticity, evidenced by

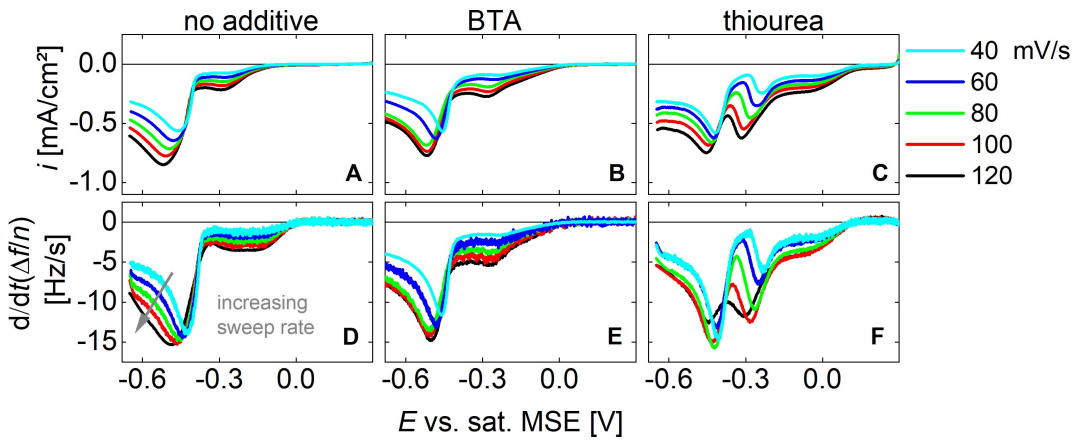

Fig. 9. Deposition sweeps on a 2.5 mM solution of $CuSO_4$ in 0.1 M H_2SO_4. Panels B, E, C and F show experiments, where plating additives (benzotriazole, BTA, and thiourea, TU) had been added at a concentration of 10 µM.

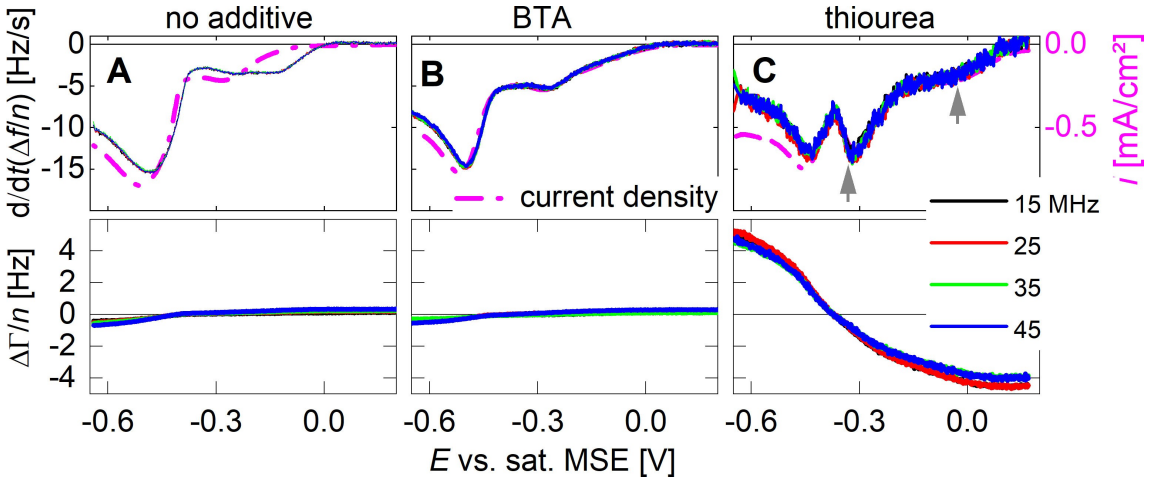

Fig. 10. A subset of the data from Figure 9 together with the electric current and the bandwidth. The sweep rate was 120 mV/s. The top panels compare the current and the apparent mass transfer rate. With the exception of the experiment with no additives, the two largely overlap. The bottom panels show the bandwidth. Addition of thiourea lets the bandwidth increase by a large amount.

shifts in ΔΓ. This layer may be interpreted as an assembly of loose aggregates. There are two separate features in the voltage range of UPD (grey arrows in Figure 10). Assigning these two peaks to specific processes would require additional structural investigations. Again, these findings apply to UPD. The influence of TU on bulk deposition at high deposition rates (common in practical plating processes) may be different.

4 Conclusions

Using a fast EQCM and exploiting accumulation, details of copper electrodeposition have become accessible with unprecedented precision. An apparent mass transfer rate can be computed from the time derivative of $\Delta f(t)/n$ and can be directly compared to the current. The current and the apparent mass transfer rate show similar features, but they differ in the quantitative details. Nanoscale roughness presumably is among the reasons. A clear non-gravimetric signal is seen in the bandwidth, which decreases during deposition. The data traces observed in UPD (with and without plating additives) display multiple peaks, steps and shoulders, the interpretation of which would require structural information. Electrogravimetry as undertaken with the modulation QCM yields datasets comparable in data quality and information content to cyclic voltammetry.

Author Contributions

Conceptualization: Johannsmann, D., Leppin, C.; Methodology: Leppin, C., Johannsmann, D.; Software: Leppin, C., Johannsmann, D.; Validation: Johannsmann, D., Leppin, C., Langhoff, A., Höfft, O.; Formal analysis: Leppin, C., Johannsmann, D.; Investigation: Leppin, C.; Resources: Johannsmann, D.; Data Curation: Leppin, C., Johannsmann, D.; Writing – Original Draft Preparation: Leppin, C., Johannsmann, D.; Writing – Review and Editing: Leppin, C., Johannsmann, D., Langhoff, A., Höfft, O.; Visualization: Leppin, C., Johannsmann, D.; Supervision: Johannsmann, D, Langhoff, A.; Project Administration: Johannsmann, D.; Funding Acquisition: Johannsmann, D. All authors have read and agreed to the published version of the manuscript.

Acknowledgements

Prof. Dr. Frank Endres, Silvia Löffelholz, and Anna Gödde from the Institute of Electrochemistry (TU Clausthal) have contributed with REM/EDX and XPS measurements. Sven Hampel (Institute of Inorganic and Analytical Chemistry (TU Clausthal) undertook GI-XRD measurements. GI-XRD was carried out at the Institute of Non-Metallic Materials (TU Clausthal). This work was in part funded by the Deutsche Forschungsgemeinschaft (DFG) under contract Jo278-19/1. Open access funding enabled and organized by Projekt DEAL.

Data Availability Statement

Data available on request from the authors.

References

[1] S. Bruckenstein, M. Shay, *Electrochim. Acta* **1985**, *30*, 1295–1300.
[2] A. R. Hillman, *J. Solid State Electrochem.* **2011**, *15*, 1647–1660.
[3] T. Nomura, M. Okuhara, *Anal. Chim. Acta* **1982**, *142*, 281–284.
[4] T. Nomura, O. Hattori, *Anal. Chim. Acta* **1980**, *115*, 323–326.

[5] L. Daikhin, V. Tsionsky, E. Gileadi, M. Urbakh, in: *Electroanalytical Chemistry: A Series of Advances*, A. J. Bard, I. Rubinstein, Eds. Marcel Dekker Inc: 2003; pp 1–99.
[6] G. L. Borges, K. K. Kanazawa, J. G. Gordon, *J. Electroanal. Chem.* **1994**. *364*, 281–284.
[7] E. J. Martin, K. Sadman, K. R. Shull, *Langmuir* **2017**, *32*, 7747–7756.
[8] A. R. Hillman, I. Efimov, K. S. Ryder, *J. Am. Chem. Soc.* **2005**, *127*, 16611–16620.
[9] A. Bund, G. Schwitzgebel, *Electrochim. Acta* **2000**, *45*, 22–23, 3703–3710.
[10] L. Daikhin, E. Gileadi, G. Katz, V. Tsionsky, M. Urbakh, D. Zagidulin, *Anal. Chem.* **2002**, *74*, 554–561.
[11] G. McHale, R. Lucklum, M. I. Newton, J. A. Cowen, *J. Appl. Phys.* **2000**, *88*, 7304–7312.
[12] R. Etchenique, T. Buhse, *Analyst* **2002**, *127*, 1347–1352.
[13] R. Funari, A. Matsumoto, J. R. de Bruyn, A. Q. Shen, *Anal. Chem.* **2020**, *92*, 8244–8253.
[14] C. Leppin, A. Peschel, F. S. Meyer, A. Langhoff, D. Johannsmann, *Analyst* **2021**, *146*, 2160–2171.
[15] R. Beck, U. Pittermann, K. G. Weil, *Ber. Bunsen-Ges. Phys. Chem* **1998**, *92*, 1363–1368.
[16] R. Fernandez, M. Calero, J. V. Garcia-Narbon, I. Reviakine, A. Arnau, Y. Jimenez, *IEEE Sens. J.* **2021**, *21*, 6643–6651.
[17] E. Gileadi, *Physical Electrochemistry: Fundamentals, Techniques and Applications.* Wiley-VCH: 2011.
[18] A. Ispas, A. Bund, Electrochemical Quartz Crystal Microbalance. In *Encyclopedia of Applied Electrochemistry*, Springer: 2014; pp 554–568.
[19] C. Gabrielli, M. Keddam, F. Minouflet, H. Perrot, *Electrochim. Acta* **1996**, *41*, 1217–1222.
[20] R. G. Compton, J. C. Eklund, F. Marken, *Electroanalysis* **1997**, *9*, 509–522.
[21] O. Schneider, S. Matic, C. Argirusis, *Electrochim. Acta* **2008**, *53*, 5485–5495.
[22] J. M. Friedt, K. H. Choi, F. Frederix, A. Campitelli, *J. Electrochem. Soc.* **2003**, *150*, H229–H234.
[23] J. Reid, *Jpn. J. Appl. Phys. 1: Regul. Pap. amp; Short Notes* **2001**, *40*, 2650–2657; Short Notes **2001**, 40, 2650–2657.
[24] D. Grujicic, B. Pesic, *Electrochim. Acta* **2002**. *47*, 2901–2912.
[25] J. W. Dini, D. D. Synder, Electrodeposition of Copper, in: Modern Electroplating **2011**. 33–78.
[26] E. Herreiro, L. J. Buller, H. D. Abruna, *Chem. Rev.* **2001**, *101*, 1897–1930.
[27] N. Mayet, K. Servat, K. B. Kokoh, T. W. Napporn, *Surfaces* **2019**, *2*, 257–276.
[28] R. Kowalik, *Arch. Metall. Mater.* **2015**, *6*, 1629–1632.
[29] E. Herrero, L. J. Buller, H. D. Abruna, *Chem. Rev.* **2001**, *101*, 1897–1930.
[30] T. Hachiya, H. Honbo, K. Itaya, *J. Electroanal. Chem.* **1991**, *315*, 275–291.
[31] B. Madry, K. Wandelt, M. Nowicki, *Appl. Surf. Sci.* **2016**, *388*, 678–683.
[32] R. J. Nichols, W. Beckmann, H. Meyer, N. Batina, D. M. Kolb, *J. Electroanal. Chem.* **1992**, *330*, 381–394.
[33] J. A. Rubio-Lara, F. Bergler, S. J. Attwood, J. M. Edwardson, M. E. Welland, *Langmuir* **2019**, *35*, 8889–8895.
[34] N. K. Allam, A. A. Nazeer, E. A. Ashour, *J. Appl. Electrochem.* **2009**, *39*, 961–969.
[35] K. Cho, J. Kishimoto, T. Hashizume, H. W. Pickering, T. Sakurai, *Appl. Surf. Sci.* **1995**, *87/88*, 380–385.
[36] D. N. Upadhyay, V. Yegnaraman, *Mater. Chem. Phys.* **2000**, *62*, 247–253.
[37] M. S. Kang, S. K. Kim, K. Kim, J. J. Kim, *Thin Solid Films* **2008**, *516*, 3761–3766.
[38] B. T. Y. Leung, M. Kang, B. F. Corry, A. A. Gewirth, *J. Electrochem. Soc.* **2000**, *147*, 3326–3337.
[39] V. Tsionsky, G. Katz, E. Gileadi, L. Daikhin, *J. Electroanal. Chem.* **2002**, *524*, 110–119.
[40] V. Tsionsky, L. Daikhin, E. Gileadi, *J. Electrochem. Soc.* **1996**, *143*, 2240–2245.
[41] A. Domack, O. Prucker, J. Ruhe, D. Johannsmann, *Phys. Rev. E* **1997**, *56*, 680–689.
[42] H. L. Bandey, S. J. Martin, R. W. Cernosek, A. R. Hillman, *Anal. Chem.* **1999**, *71*, 2205–2214.
[43] M. V. Voinova, M. Rodahl, M. Jonson, B. Kasemo, *Phys. Scr.* **1999**, *59*, 391–396.
[44] R. Lucklum, C. Behling, R. W. Cernosek, S. J. Martin, *J. Phys D* **1997**, *30*, 346–356.
[45] M. Urbakh, L. Daikhin, *Phys. Rev. B* **1994**, *49*, 4866–4870.
[46] I. Efimov, A. Ispas, A. Bund, *Electrochim. Acta* **2014**, *122*, 16–20.
[47] A. Bund, O. Schneider, V. Dehnke, *Phys. Chem. Chem. Phys.* **2002**, *4*, 3552–3554.
[48] K. Rechendorff, M. B. Hovgaard, M. Foss, F. Besenbacher, *J. Appl. Phys.* **2007**, *101*, DOI: 10.1063/1.2735399.
[49] T. C. Girija, M. V. Sangaranarayanan, *J. Solid State Electrochem.* **2005**, *9*, 621–626.
[50] H. D. B. Jenkins, Y. Marcus, *Chem. Rev.* **1995**, *95*, 2695–2724.
[51] L. T. Viyannalage, R. Vasilic Dimitrov, *J. Phys. Chem. C* **2007**, *111*, 4036–4041.
[52] F. Grillo, H. Früchtl, S. M. Francis, N. V. Richardson, *New J. Phys.* **2011**, *13*, 013044.
[53] A. J. Bard, L. R. Faulkner, "Electrochemical Methods: Fundamentals and Applications" (2nd ed.) John Wiley & Sons 2001.
[54] G. J. Hills, D. J. Schiffrin, J. Thompson, *Electrochim. Acta* **1974**, *19*, 657–670.
[55] M. J. Armstrong, R. H. Muller, *J. Electrochem. Soc.* **1991**, *138*, 2303–2307.
[56] J. C. Farmer, *J. Electrochem. Soc.* **1985**, *132*, 2640–2648.

Received: August 16, 2021
Accepted: September 16, 2021
Published online on October 7, 2021

